fib Congress 2026
Lisbon - Portugal

Crack Monitoring during Load Testing of Full-Scale Dapped-End RC Beams with Varying Reinforcement Layouts

Luke van Ratingen[1,*], Andras Vanquaille[2], Nadia Amin[3], Els Verstrynge[4], Boyan Mihaylov[5], Eline Vereecken[6], Hervé Degée[7]

1. Ing. Construction Engineering Research Group, Hasselt University, Diepenbeek, Belgium
2. Ir. Arch. Materials and Constructions Division, Civil Engineering Department, KU Leuven, Leuven, Belgium
3. Ir. Urban and Environmental Research Unit (UEE), Univ. of Liège, Liège, Belgium
4. Prof. Dr Ir. Arch. Materials and Constructions Division, Civil Engineering Department, KU Leuven, Leuven, Belgium
5. Prof. Dr Ir. Urban and Environmental Research Unit (UEE), Univ. of Liège, Liège, Belgium
6. Prof. Dr Ir. Construction Engineering Research Group, Hasselt University, Diepenbeek, Belgium
7. Prof. Dr Ir. Construction Engineering Research Group, Hasselt University, Diepenbeek, Belgium

[*]Corresponding author email: luke.vanratingen@uhasselt.be

Abstract

Reinforced concrete structures from the 1970s and 80s are reaching the end of their service life, with critical zones, such as dapped-end (DE) regions found in Gerber-type bridges, showing increased vulnerability to deterioration. These regions, characterised by geometric discontinuities, are prone to damage due to the combined effects of mechanical loading, consequent cracking, and environmental exposure. As part of a larger research project investigating the interaction between corrosion, sustained loading and mechanical resistance, this study presents the first experimental phase, focused on the short-term mechanical behaviour of full-scale DE beams and, in particular, on the development of the crack patterns. The primary objective of this phase is to establish a reliable mechanical reference for the subsequent long-term experimental campaigns, which will encompass corrosion and creep effects. A combination of traditional and advanced measurement techniques was used during testing, including strain gauges, linear variable differential transducers (LVDT or LT) and crack width monitoring. These tools enabled high-resolution tracking of crack development, strain distribution, and bond-slip behaviour in the critical DE zones. Subsequently, the results from this initial test series are used to validate finite element models for these complex regions.

Keywords: *Dapped-end beams, Reinforced concrete, Corrosion, Static testing, Failure mechanisms*

1. Introduction

A large proportion of reinforced concrete bridge infrastructure in Europe was constructed during the 1970s and 1980s and is currently approaching or exceeding a service life of approximately 50 years. For many of these structures, deterioration processes such as reinforcement corrosion, concrete cracking, and material ageing are becoming increasingly critical, raising concerns regarding structural safety and long-term durability. Several high-profile bridge collapses in recent decades have demonstrated that local weaknesses in critical structural details can trigger the global failure of entire bridge systems. Notable examples include the collapse of the de la Concorde overpass in Canada (Gouvernement du Québec 2007) and the Annone Brianza bridge collapse in Italy (D'Angelo et al. 2025). These events highlight the urgent need for improved assessment tools and experimentally validated evidence to support decision-making for ageing bridge infrastructure. One structural detail that has proven particularly vulnerable is the reinforced concrete dapped-end (DE) beam, which is commonly used in Gerber-type bridge systems (Fig. 1). Dapped ends introduce a geometric discontinuity that results in highly non-uniform stress distributions and pronounced tensile stress concentrations near the re-entrant corner. Therefore, under service loading conditions, this region is prone to early crack opening of wide cracks. Once formed, these cracks act as preferential pathways for water and chlorides, significantly accelerating reinforcement corrosion and the associated degradation of load-bearing capacity. Field inspections of existing bridges in Belgium and elsewhere have repeatedly identified severe cracking and advanced corrosion damage in dapped-end regions, often at a critical stage.

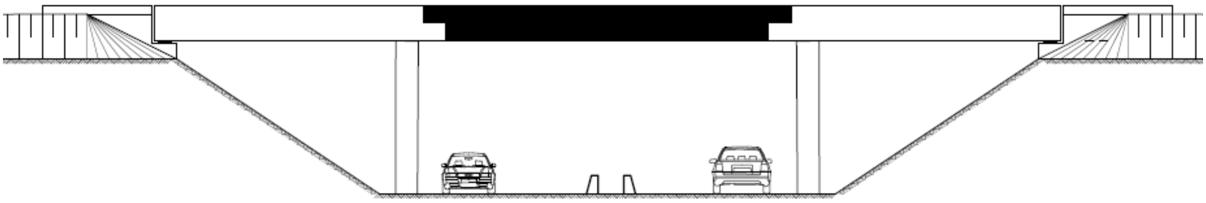

Figure 1. Gerber-type bridge design with DE-beams

Previous experimental and analytical research performed by Rajapakse et al. (2022, 2023) and Desnerck et al. (2014, 2016, 2017) has substantially improved the understanding of the mechanical behaviour of dapped end beams under monotonic loading, identifying characteristic failure mechanisms of DE beams such as brittle shear failure, ductile shear failure, and flexural failure. In particular, earlier large-scale experimental campaigns conducted at UHasselt and ULiège by Rajapakse (2023) have demonstrated that a significant proportion of failures in lab tests is directly linked to the initiation and propagation of the re-entrant corner crack. However, most available studies focus on specimens without pre-existing damage and do not consider the interaction between mechanical loading, time dependent effects, and corrosion induced degradation. Experimental data capturing this coupled behaviour therefore remain scarce, despite their clear relevance for the assessment of existing bridge infrastructure.

The current experimental program is structured in multiple phases. An initial phase consists of short-term static tests on full-scale DE beams in normal (non-corrosive) conditions, followed by long-term creep tests under sustained loading, and subsequent corrosion tests under combined sustained loading and chloride exposure. Each phase concludes with static loading to failure, enabling a direct comparison of residual strength and failure mechanisms after long-term degradation. The primary objective of the first phase, reported in this contribution, is to establish a reliable mechanical reference for the behaviour of full-scale dapped-end beams prior to the introduction of time-dependent and environmental effects. Emphasis is placed on the load-deformation response, the development of characteristic crack patterns, particularly at approximately 50% of the ultimate load, and the identification of governing failure mechanisms. In addition, the experimental results from this first phase are used to validate finite element analyses (FEA) performed with DIANA FEA (2023) for later parametric studies. Comparisons between experimentally observed load-displacement curves and corresponding numerical predictions are presented to assess the models' ability to reproduce the observed global behaviour. Detailed local phenomena associated with the re-entrant corner crack, as well as in-depth material degradation effects, will not be discussed in this contribution. By providing a clear experimental baseline for the mechanical performance of dapped-end beams in normal conditions, this paper aims to set the stage for the interpretation of future creep and corrosion tests and to contribute to a more reliable assessment of ageing RC bridge infrastructure.

2. Experimental programme and test specimens

2.1. Test setup and instrumentation

The experimental setup for the static tests up to failure is similar to that previously employed by Rajapakse (2023), as illustrated in Figure 2. This approach enables a direct comparison between the results of the present study and earlier experimental data. In addition, the same measurement layout has been adopted, including a comparable arrangement of LTs, manual crack width measurements with a digital microscope camera between load increments, and strain gauges on the rebars.

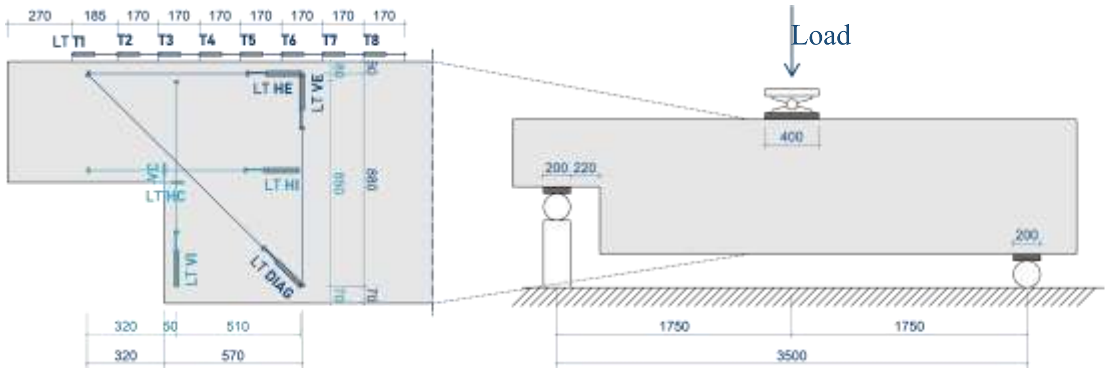

Figure 2. Test setup and instrumentation position in mm retrieved from Rajapakse (2023)

In contrast to earlier experimental studies on dapped-end beams conducted at UHasselt and ULiège, which used beams with dapped ends at both extremities, the present study utilises beams with a single-sided dapped end. The opposite end of the beam is configured as a straight end, with the central longitudinal reinforcement bars intentionally extending beyond the concrete surface to allow for the attachment of measurement equipment. For the current experimental series, the overall dimensions of the test specimens are selected to ensure support conditions identical to those adopted in the tests previously conducted by Rajapakse (2023) at UHasselt and ULiège.

2.2. Test specimens and reinforcement layouts

The experimental programme focuses on full-scale DE beams representative of bridge construction practice from the 1970s and 1980s, during which orthogonal reinforcement layouts were commonly applied in dapped-end regions. Three reinforcement amounts were selected to reflect the range typically encountered in existing infrastructure (Fig. 2). The selected configurations are based on those previously investigated by Rajapakse (2023) and Hippola and Mihaylov (2025) for dapped-end beams with orthogonal reinforcement layouts characteristic of that period. Based on the amount of reinforcement provided in the dapped-end region, the beams are classified as lightly reinforced (L), moderately reinforced (M), and heavily reinforced (H). Concrete material properties were measured from compressive strength tests on three concrete cubes, as well as compressive strength and Young's modulus tests conducted on three concrete cylinders, as shown in Table 1.

Table 1. Beam identification and concrete properties.

Beam type	Reinforcement level	Name	$f_{c,cyl}$ [MPa]	E_c [MPa]
L	Low	RE-L	46.2 (5.6)	43 667 (13.6)
M	Moderate (standard)	RE-M	41.7 (20.3)	39 100 (5.6)
H	High	RE-H	41.3 (7.2)	35 433 (0.9)

Beam RE-L represents the specimen with the lowest level of shear reinforcement. In the full-depth region close to the dapped end, shear reinforcement is limited to three sets of four-legged Ø8 stirrups, while the stirrup spacing in the remainder of the full-depth portion is increased compared to the other beam types, reinforcement layouts are illustrated in figure 3. This results in a reduced overall shear reinforcement ratio in the critical region. Beam RE-M has a reinforcement configuration that is more balanced relative to the concrete capacity. In the region close to the dapped end and the re-entrant corner, five sets of closely spaced four-legged Ø10 stirrups are provided, increasing confinement and shear resistance. Further away from the dapped end, the full-depth region is reinforced with two-legged Ø12 stirrups at shorter spacing, corresponding to conventional shear reinforcement in the remainder of the beam. Beam RE-H contains the highest level of shear reinforcement among the tested beams. The number and spacing of stirrups in the dapped-end and re-entrant corner region are identical to those of beam RE-M. However, the stirrup diameter in this region is increased to Ø12, matching that of the stirrups used in the full-depth portion of the beam. This further enhances shear capacity and confinement in the critical region, targeting a switch to a bending failure mode.

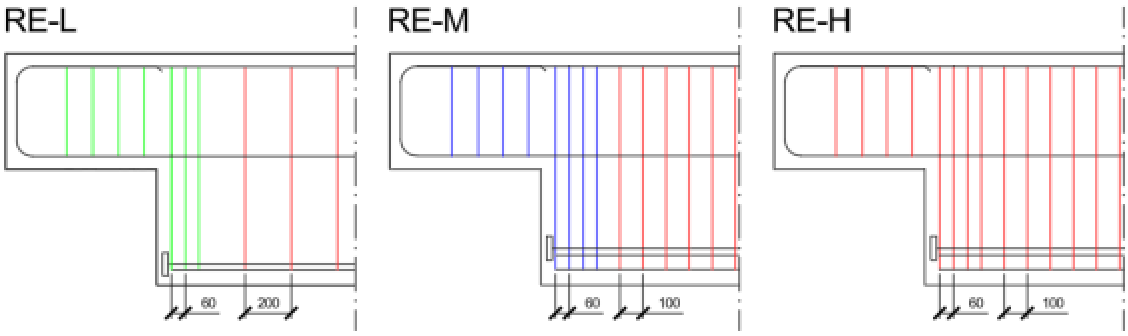

Figure 3. Construction drawing dapped-end beams; RED = ø 12, BLUE = ø 10, GREEN = ø 8

A key modification relative to earlier experimental campaigns concerns the detailing of the shear reinforcement. In the present study, the number of stirrups has been increased and a uniform stirrup diameter is adopted throughout the beam. Whereas the original design incorporated stirrups with varying diameters (Ø8, Ø10, and Ø12), all beams in this programme employ a consistent stirrup diameter of 12 mm over the full beam depth. Within the dapped-end region, and particularly in the zone of high stress concentration near the re-entrant corner crack, variations in stirrup detailing are retained to reflect local reinforcement demands. Additional stirrups are provided in the dapped-end region and placed closer to the re-entrant corner crack, as illustrated in Figure 3, to ensure adequate confinement and to investigate the influence of stirrup detailing on crack development and failure behaviour.

Tensile tests were conducted on the reinforcing steel to determine its mechanical properties. For each bar diameter, three specimens were tested in tension. The average values of the yield strength, ultimate tensile strength Young's modulus and rupture strain are reported in Table 2 below and are used throughout this study for the interpretation of the experimental results.

Table 2. Average mechanical properties of reinforcing steel. The coefficient of variation (CV), expressed as a percentage, is given in parentheses for averaged quantities; ε_r is reported as the measured range.

Bar diameter	$f_{y,avg}$ **[MPa]**	$f_{u,avg}$ **[MPa]**	E_{avg} **[MPa]**	ε_r [‰]
Ø8	469 (3.8)	568 (0.1)	194 490 (3.4)	14-20
Ø10	522 (1.5)	650 (0.1)	214 530 (13.3)	114-120
Ø12	535 (1.6)	653 (0.1)	175 480 (6.7)	95-108
Ø14	547 (2.9)	672 (0.1)	206 800 (2.4)	106-114
Ø16	604 (0.5)	731 (0.3)	204 560 (10.7)	75-85
Ø20	523 (1.3)	667 (0.3)	215 360 (14.2)	110-112

3. Experimental setup and monitoring strategy

3.1. Test Configuration and Loading Protocol

The static tests were performed under controlled laboratory conditions using a loading configuration intended to replicate the force transfer mechanisms typical of dapped-end regions in Gerber-type bridge systems, as illustrated in Figure 3. The load was applied in a stepwise manner with constant increments of 100 kN until failure, allowing intermediate inspection of crack development and deformation behaviour. Up to a load level of 500 kN, each increment was followed by partial unloading corresponding to 10% of the applied load to enable manual crack measurements, while beyond 500 kN unloading was performed by reducing the load by a fixed amount of 50 kN. This loading–unloading sequence was continued until unstable behaviour was observed, after which crack measurements were discontinued and loading was continued monotonically until failure.

3.2. Monitoring Strategy

A comprehensive monitoring strategy was implemented to capture both global and local structural response throughout the test. LTs were primarily used to measure global displacements and diagonal deformations, which govern the beam's overall force–displacement response. In total, fifteen LTs were installed. Of these, eight were arranged in a linear configuration along the top surface of the beam to monitor the concrete cover's compression and deformation. Five additional LTs were positioned to capture global surface deformations, while two smaller LTs were placed in the vicinity of the re-entrant corner to monitor crack opening and local displacement behaviour (Fig. 2). Strain gauges were used to complement the LT measurements. Strain gauges were installed on selected stirrups and longitudinal reinforcement bars, before concrete casting, to record internal strain development. Manual crack width measurements were performed during each load step using a high-resolution crack camera.

4. Experimental results: global mechanical behaviour

4.1. Force-displacement response

All three beams were tested individually under static loading until failure. Figure 4 presents the force–displacement response obtained from the diagonal LT measurements, providing an overview of the global mechanical behaviour of the three beam types and the governing deformation of the dapped-end region. All specimens exhibited a predominantly ductile response governed by yielding of the reinforcement in the re-entrant corner crack; however, the beam with the highest reinforcement ratio showed reduced ductility due to increased compression demands on the concrete. With regard to the subsequent phases of the research programme, particularly the creep and corrosion experiments, load levels corresponding to approximately 50% of the ultimate capacity are of primary interest. This load level is considered representative of long-term service conditions and is associated with crack widths favourable for capillary suction during corrosion exposure. The static tests, therefore, served to establish reliable reference values for the load-bearing capacity of each beam type and to relate applied load levels to the corresponding structural response.

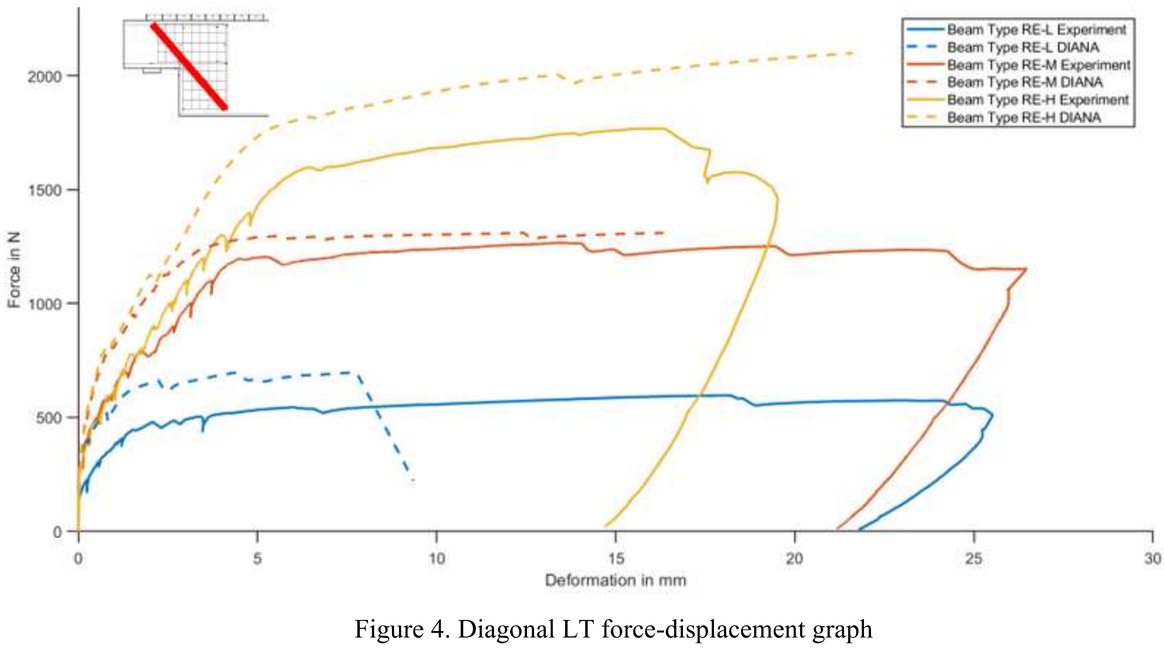

Figure 4. Diagonal LT force-displacement graph

4.2. Crack development and failure mechanisms

Crack development was monitored during loading, focusing on crack patterns and widths at approximately 50% of the ultimate load, which is relevant for specimen comparison and subsequent creep and corrosion tests. Eurocode 2 (2023) provides guidance on crack control by specifying a maximum allowable crack width of 0.3 mm for durability under serviceability limit state conditions. This value is used as a normative reference for assessing crack development in the tested beams. Experimental evidence indicates that wider cracks are particularly relevant for corrosion studies. Poursaee (2022) reports that crack widths in the range of approximately 0.3–0.7 mm are favourable for capillary suction of moisture and chlorides in cracked concrete. Based on these findings, this crack width range is targeted during the corrosion phase of the experimental programme. The static test results are therefore used to identify the load levels at which these crack widths are attained for each beam type. The failure modes are also documented and related to the intended governing failure mechanisms associated with the different reinforcement layouts.

4.2.1. Beam RE-L

At 50.2% of the peak load corresponding to a load level of 300 kN for beam RE-L the observed damage state is presented in Figure 5. At this stage of the test, a dominant crack had developed at the re-entrant corner, with a measured maximum crack width of 0.8 mm near the concrete surface. With continued loading, crack widening and propagation intensified, ultimately leading to failure at a maximum load of 597.4 kN. The beam failed due to yielding of the horizontal and vertical reinforcement in the re-entrant corner crack, which caused large plastic rotations of the dapped end about the tip of the crack. The failure load was also affected by rupture of some of the vertical reinforcement in the critical corner crack, which initiated at a load of approximately 480 kN. This failure mode can be described as flexural, as it occurred along the re-entrant corner crack with rotations of the dapped end relative to the full-depth section (Fig. 6).

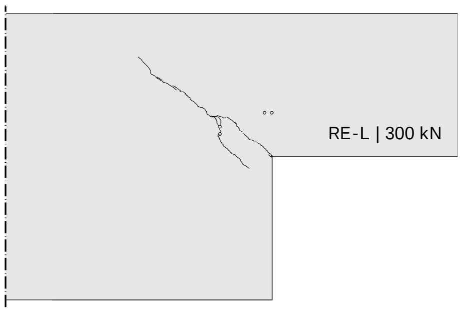

Figure 5. RE-L crack pattern at approx. 50% peak load

Figure 6. RE-L crack pattern at failure

4.2.2. Beam RE-M

At 55.3% of the peak load, corresponding to a load level of 700 kN for beam RE-M, the crack pattern observed in the dapped end region is shown in Figure 7. At this stage of the test, cracking was more distributed than in beam RE-L, while a clearly developed re-entrant corner crack was present. The measured crack width at this load level was 0.56 mm. With continued loading, crack propagation and widening intensified, ultimately leading to failure at a maximum load of 1266.5 kN. As evident from Figure 8, similarly to specimen RE-L, this dapped end failed with plastic rotations in the re-entrant corner crack caused by yielding of the horizontal and vertical reinforcement in the crack. Crushing of concrete in the compression zone on the top side of the specimen, as well as ruptures of vertical reinforcement occurred along the plastic plateau of the force-displacement response. These effects limited the ductility of the specimen but did not affect significantly its the peak resistance (strength). This failure mode can also be classified as flexural, even though the crushing of the concrete may have been affected by a shear crack from the dapped end. It can be seen in Figure 8 that the crack extended from the inner edge of the loading plate and penetrated the compression zone.

Figure 7. RE-M crack pattern at approx. 50% peak load

Figure 8. RE-M crack pattern at failure

4.2.3. Beam RE-H

At 50.9% of the peak load, corresponding to a load level of 900 kN for beam RE-H, the crack pattern observed in the dapped end region is shown in Figure 9. At this load level, a significantly larger number of shear cracks had developed compared to beams RE-L and RE-M, extending not only in the dapped end region but also into the full depth of the beam. This indicates a more distributed shear cracking response, associated with the increased reinforcement. The measured crack width at the re-entrant corner at this load level was 1.01 mm. With continued loading, the beam reached a maximum load of 1768 kN, at which failure occurred due to spalling of the top concrete cover on the top face of the beam, as illustrated in Figure 10. Regardless of the high amount of reinforcement crossing the re-entrant corner crack, the main horizontal and vertical reinforcement yielded in the crack prior to failure. However, compared to specimen RE-M, the concrete in the compression zone crushed earlier along the plastic plateau of the force-displacement response, and the reinforcement did not reach rupture. Concrete cover spalling was also observed at the top of the specimen. Because the re-entrant corner crack and the shear cracks in the dapped end were rather diffused at failure, this failure mode can be characterized as mixed flexural-shear mode.

Figure 9. RE-H crack pattern at approx. 50% peak load

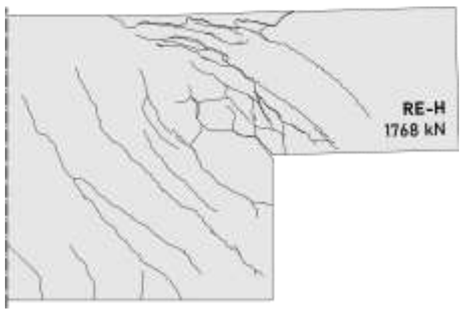

Figure 10. RE-H crack pattern at failure

5. Comparison with numerical modelling

5.1. Finite element modelling approach

Finite element analyses (FEA) were conducted using the DIANA FEA (2023) software package. The numerical models were developed to replicate the experimental test setup and incorporate material properties obtained directly from the experimental program, as summarised in Tables 1 and 2. 2 D models were developed for each beam layout used, as shown for the RE-H beam in figure 11. Concrete was modelled using a nonlinear constitutive framework. The tensile behaviour was described by the Hordijk tension softening model, while a parabolic stress–strain relationship was adopted for compression. Compression softening was accounted for using the model of Vecchio and Collins, and confinement effects were included following Selby and Vecchio. Reinforcing steel was modelled using a nonlinear von Mises plasticity formulation. Where relevant, bond–slip behaviour between reinforcement and concrete was represented by an interface model based on Doerr. The Doerr interface model in DIANA FEA represents steel–concrete bond–slip behaviour using zero-thickness interface elements governed by a non-linear bond stress–slip relationship. The numerical results were validated through direct comparison with experimentally measured load-displacement responses. In addition, reinforcement strains were extracted at locations corresponding to the strain gauges, enabling validation of the simulated strain development against experimental observations.

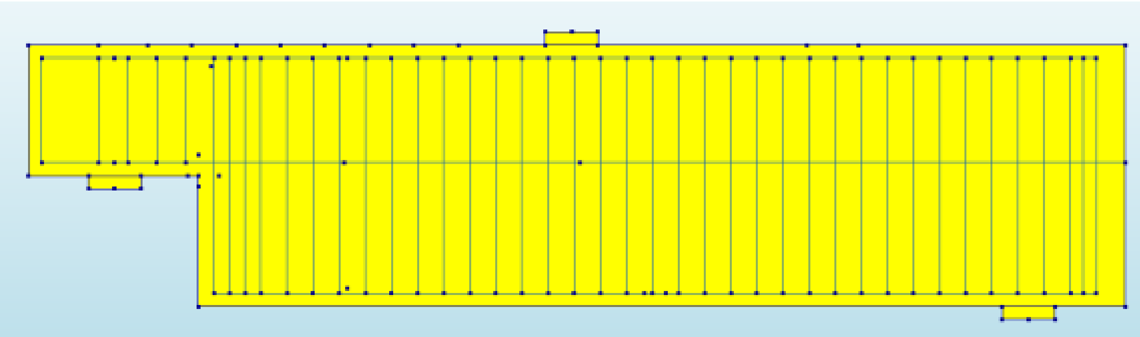

Figure 11. DIANA FEA model of the RE-H beam

5.2. Experimental–numerical comparison

Figure 4 compares the experimentally measured diagonal LT response of beam RE-M with the corresponding digital LT output obtained from the DIANA finite element model. Overall, good agreement is observed between the experimental and numerical force-displacement responses, indicating that the numerical model captures the beams' global mechanical behaviour. The DIANA models exhibit a higher initial stiffness than the experiments, as reflected by the steeper slope at small displacements. This difference can be attributed to modelling idealisations, such as the assumption of a perfect bond and the absence of initial microcracking due to shrinkage and construction-related imperfections present in the experimental specimen. The experimental response is influenced by the stepwise loading protocol with partial unloading at each load level, resulting in local load drops and stiffness changes. These effects are not captured in the numerical simulations, which were performed under monotonic loading conditions, resulting in a smoother numerical response. The DIANA model slightly overestimates the peak load of all the tested beams, while still reproducing the overall trend of the force-displacement behaviour. In the post-peak range, the numerical response remains relatively stable compared to the experimental response, which shows more pronounced degradation due to crack localisation, local damage, and repeated unloading. Despite these differences, the diagonal deformation obtained from the DIANA model provides an adequate representation of the global diagonal extension of the dapped end. However, additional improvement of the DIANA model is required.

6. Discussion and conclusions

The experimental programme demonstrates clearly how the amount and detailing of orthogonal reinforcement in the dapped-end region governs crack development, load-carrying capacity and the ultimate failure mechanism of full-scale beams. A systematic evolution in structural response is observed from beam RE-L to RE-H, reflecting the transition from reinforcement-controlled behaviour towards concrete-governed limitations. At service-relevant load levels around 50% of the ultimate capacity, all specimens exhibited pronounced cracking at the re-entrant corner, confirming this region as the critical location for both structural performance and durability. However, the crack patterns and widths differed significantly.

Beam RE-L showed early crack localisation, with a dominant re-entrant corner crack reaching relatively large widths. This localised response reflects the limited amount of reinforcement and resulted in a flexural failure mechanism governed by yielding and partial rupture of the reinforcement crossing the corner crack, accompanied by large plastic rotations of the dapped end (Fig. 12).

In beam RE-M, the enhanced reinforcement led to a more distributed cracking response in the dapped-end region and a substantial increase in load-carrying capacity. Although a clearly defined re-entrant corner crack still governed the behaviour, crack development was more gradual and the specimen exhibited an extended plastic plateau. Failure was again flexural in nature, controlled by reinforcement yielding in the corner crack, while concrete crushing in the compression zone and local reinforcement rupture reduced ductility without significantly affecting peak strength (Fig 13).

For beam RE-H, the further increase in reinforcement resulted in a markedly different response. Crack patterns became more diffuse, with multiple shear cracks extending from the dapped end into the full-depth section. Despite yielding of the reinforcement at the re-entrant corner, failure was governed by concrete-related mechanisms, including early crushing of the compression zone and spalling of the concrete cover. As a result, the ultimate behaviour can be classified as a mixed flexural–shear failure mode, in which the concrete capacity rather than the reinforcement strength became the limiting factor. The reduced ductility observed for this specimen indicates that increasing reinforcement beyond a certain level does not necessarily enhance structural robustness (Fig 14).

Figure 12. Failure of RE-L

Figure 13. Failure of RE-M

Figure 14. Failure of RE-H

The comparison between experimental measurements and DIANA finite element simulations shows that the numerical model captures the global force–displacement behaviour with reasonable accuracy. Stiffness, non-linear response and ultimate load levels are reproduced satisfactorily, although a slight overestimation of the peak resistance is observed. Differences in initial stiffness and response smoothness are attributed to modelling idealisations and the monotonic loading assumption, whereas the experiments involved stepwise loading with partial unloading. While the numerical model is adequate for assessing global behaviour, the results highlight the need for caution when interpreting local damage evolution, crack localisation and post-peak behaviour using continuum-based approaches. Overall, the experimental and numerical findings form a robust reference framework for long-term investigations on dapped-end beams. Future research will focus on extending the numerical modelling approach to incorporate time-dependent effects such as creep and corrosion-induced degradation, and on validating these models against long-term experimental observations. Special attention will be given to the interaction between sustained loading, crack width evolution and reinforcement corrosion in the re-entrant corner region, which has been confirmed as the governing zone for both structural performance and durability.

Acknowledgements

The authors gratefully acknowledge the financial support of the Research Foundation – Flanders (FWO) under project number G0A3H24N. The experimental work was carried out in the ACB² laboratory at Hasselt University. The authors further acknowledge the collaboration with KU Leuven and the University of Liège, whose expertise in materials, structural behaviour, and numerical modelling significantly contributed to the execution and interpretation of the research.

References

Desnerck, P., Lees, J.M., and Morley, C. (2014). Assessment of reinforced concrete half-joint structures: dealing with deterioration. Proceedings of the 2014 PCI Convention and National Bridge Conference, 16 pp.

Desnerck, P., Lees, J.M., and Morley, C.T. (2016). Reinforcement layout implications for reinforced concrete half-joint structures. Engineering Structures, 127, 227–239.

Desnerck, P., Lees, J.M., and Morley, C.T. (2017). The effect of local reinforcing bar reductions and anchorage zone cracking on the load capacity of RC half-joints. Engineering Structures, 152, 865–877.

DIANA FEA BV (2023). DIANA Finite Element Analysis, User's Manual. Delft, The Netherlands.

D'Angelo, M., Civera, M., Giordano, P.F., Borlenghi, P., Ballio, F., Limongelli, M.P., and Chiaia, B. (2025). Bridge collapses in Italy across the 21st century: Survey and statistical analysis. Structure and Infrastructure Engineering. DOI: 10.1080/15732479.2025.2483500.

EN 1992-1-1 (2023). Eurocode 2: Design of concrete structures – Part 1-1: General rules and rules for buildings.

Gouvernement du Québec (2007). Report on the de la Concorde Overpass Collapse: Causes and Recommendations. Canadian Electronic Library, Canada. DOI: 20.500.12592/7md68x.

Hippola, S., and Mihaylov, B. I. (2025). Experimental investigation of the fatigue behaviour of reinforced concrete dapped-end connections. Proceedings of the fib Symposium, Fédération Internationale du Béton (fib).

Poursaee, A., and Ross, B. (2022). The role of cracks in chloride-induced corrosion of carbon steel in concrete—Review. Corrosion and Materials Degradation, 3, 258–269.

Rajapakse, C. (2023). Behaviour and Modelling of Reinforced Concrete Dapped-End Connections. PhD Thesis, University of Liège and Hasselt University, Belgium.

Rajapakse, C., Degée, H., and Mihaylov, B. (2022). Investigation of shear and flexural failures of dapped-end connections with orthogonal reinforcement. Engineering Structures, 260, 114233.